Ultrasound monitoring for evaluation of damage in reinforced concrete

M. RUCKA* and K. WILDE

Department of Structural Mechanics, Faculty of Civil and Environmental Engineering,
Gdansk University of Technology, 11/12 Narutowicza St., 80-233 Gdańsk, Poland

Abstract. The paper deals with automated monitoring of damage evolution in concrete elements subjected to three-point bending tests. The monitoring is based on the nonlinear interactions of traveling ultrasonic waves with micro-crack zones inside the concrete specimens and surface-breaking cracks. The developed procedure assumes semi-continuous ultrasonic testing during the element full loading cycle and generation of the power spectral density maps for the on-line assessment of the degradation process. Two damage indicators are introduced to evaluate micro- and macro-damage. The preliminary experimental results show that the proposed automated monitoring system provides an effective method for the evaluation of progressive damage in concrete.

Key words: concrete, degradation, micro-cracking, non-destructive evaluation, ultrasonic waves.

1. Introduction

The material and structural parameters of concrete structures vary in time due to inevitable aging. Damage in concrete occurs as a result of overloading, shrinkage, temperature, chemical attacks or fatigue. Surface-breaking cracks belong to the most commonly encountered kind of defects in civil engineering structures [1]. Before an open crack (macro-crack) emerges, zones of micro-cracks of size not larger than aggregate size develop within a concrete element. Detection of such micro-scale damage is not a trivial task and it is of great interest in civil engineering.

There are numerous non-destructive testing (NDT) methods currently applicable to the evaluation of concrete structures, e.g. acoustic emission [2–4], infrared thermography [5, 6] or ground penetrating radar [7, 8]. The techniques of particular interest concern various aspects of the elastic wave propagation [9, 10] including the impact-echo method [11] and the Lamb wave modes [12]. A standard non-destructive technique is based on non-automatic, periodic measurements. The methodology assumes that the in-situ measurements are conducted according to a regular schedule, for example once a year. The data are analysed after the inspection and then conclusions about the structure condition are drawn by an experienced engineer. The measurements and the damage detection methodologies are the most difficult tasks and they can be improved by automation of procedures.

Recent studies have highlighted a novel approach to the non-destructive evaluation of concrete based on the continuous monitoring technology applied at all stages of a structure life. Ultrasonic techniques have been proposed for monitoring and controlling the time-varying degradation of mechanical properties of concrete. Antonaci et al. [13] monitored a damage process induced by applying a mono-axial compressive load along the longitudinal direction of a cylindrical concrete specimen. After reaching each load level the specimen was removed from the loading frame and a burst of 10 sinusoidal cycles at a frequency of 55.5 kHz was propagated through the specimen. Shah and Ribakov [14] conducted ultrasonic evaluation of cube concrete specimens under uniaxial compression stepped loading. The damage assessment was performed by the analysis of the reduction in the amplitude of the waveforms transmitted through the specimen at different power levels. The evaluation of thermal damage in concrete by the nonlinear ultrasonic method was investigated by Yim et al. [15]. Cylindrical samples were exposed to temperature up to $600°C$. After cooling to temperature of $20°C$, samples were subjected to the impact-modulation method that combined the propagation of a sinusoidal continuous signal of frequency of 180 kHz with low-frequency vibrations induced by a hammer and registered by an accelerometer. Molero et al. [16] applied ultrasonic imaging to evaluate damage in concrete cylindrical samples subjected to freeze–thaw cycles. The results of monitoring of self-healing in concrete are shown in the paper by In et al. [17]. The experiments were conducted on tensile through-thickness cracked and flexure partial-thickness cracked concrete specimens. The specimens with cracks were subjected to axial load by applying prestressing force to control the crack widths and ponded with seawater solution for 120 days to initiate self-healing. Next two transducers placed on both sides of the crack were used for ultrasonic measurements. Generally speaking, research on the evaluation of damage in concrete specimens under bending load is limited to acoustic emission methods [18] or combined AC impedance and ultrasonic methods [19]. Recently Adhikari et al. [20] have presented automated crack detection in bending beams using digital images.

*e-mail: mrucka@pg.gda.pl

M. Rucka and K. Wilde

The present study focuses on monitoring of development of micro-crack zones as well as surface-breaking cracks in concrete specimens subjected to bending. This work continues previous research on monitoring of splitting failure of concrete specimens in tension [21]. The current experiments of the preliminary character have been conducted on concrete cuboid specimens that resemble beams. The specimens were reinforced with two ribbed steel bars. Complexity of concrete structures as well as heterogeneity of the material makes the interpretation of an ultrasonic wave propagation signal very difficult. Therefore, there is a need of automatic control in the process of continuous monitoring at all stages of load application to detect micro-scale damage before it develops into open cracks. The monitoring is based on the nonlinear interactions of the traveling ultrasonic waves with the micro-crack zones inside the concrete specimens as well as the surface cracks. The applied procedure assumes semi-continuous ultrasonic testing during the element full loading cycle. Two damage indicators are introduced for a continuous evaluation of damage using the proposed automated inspection system.

2. Concept of automated diagnostic system

The proposed automated diagnostic system is dedicated to monitoring of damage evolution in concrete structural elements subjected to service loads during the whole structure life-time. The system uses piezoelectric (PZT) transducers permanently mounted to the concrete element. The PZT transducers are utilized for both generation and registration of ultrasonic waves. The signals from the PZT transducers are registered in a data acquisition system and processed by a computer. The parameters of an excited wave packet (i.e. the number of counts in a tone burst and the wave frequency) as well as the threshold value are set manually before the system is activated.

The standard operation of the system assumes automatic generation and registration of ultrasonic waves propagating through the concrete element. The power spectral density (PSD) of each signal is computed just after the measurement is completed. Next a damage index informing about the appearance of micro-cracking zones is computed and an automatic warning is issued. In addition, the appearance of new dominant frequencies in the PSD is traced and an index dedicated to structural macro-damage is computed. The information based on the second index is send with a warning about potential structural damage within the concrete element. Figure 1 illustrates the concept of the automated diagnostic system for evaluation of damage evolution in reinforced concrete. In the paper the proposed diagnostic system is laboratory tested on the example of the reinforced concrete specimens subjected to monotonically increasing loading.
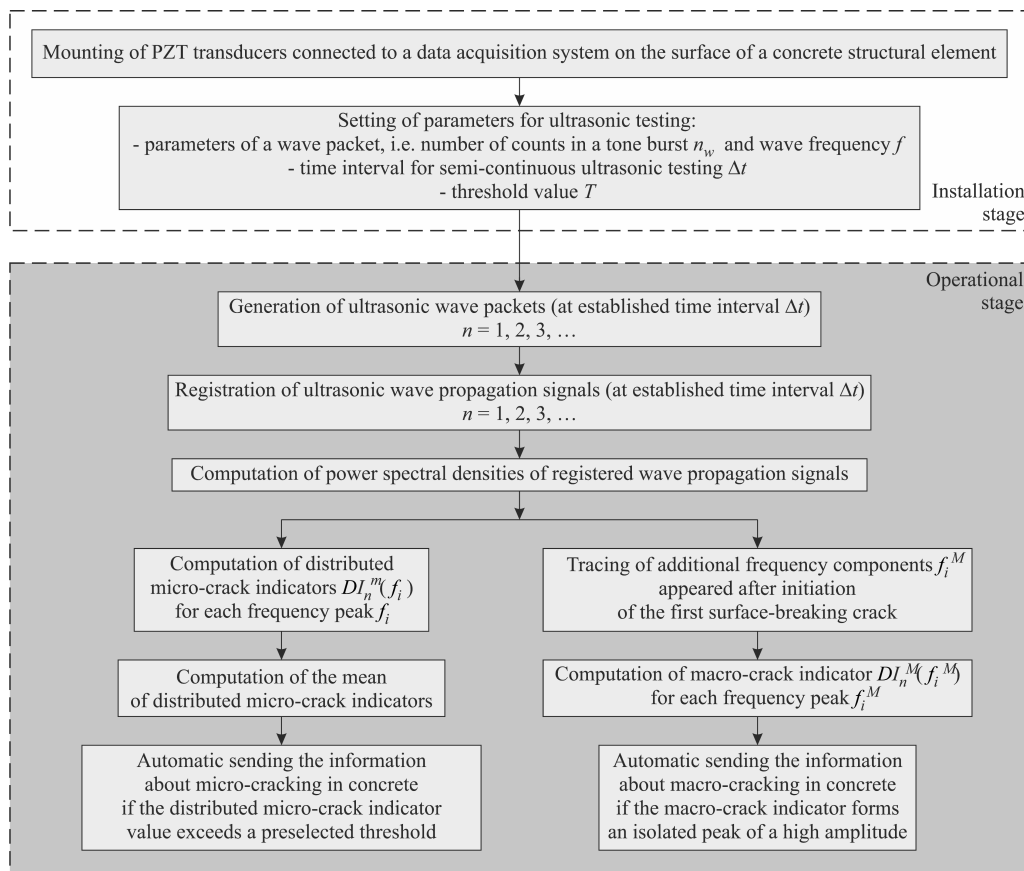

Fig. 1. Schematic diagram illustrating the concept of the automated diagnostic system for evaluation of damage evolution in reinforced concrete

3. Experimental setup

3.1. Description of specimens. The tested samples were rectangular prisms with a cross-section of 10 cm × 15 cm and a length of 50 cm (Fig. 2) made of concrete of quality C20/25. The ingredients of concrete were: Portland cement type CEM I 42.5R (240 kg/m³), sand 0–2 mm (819 kg/m³), fine aggregate 2–8 mm (260 kg/m³), coarse aggregate 8–16 mm (680 kg/m³), ash (85 kg/m³), superplasticizers (3.41 kg/m³) and water (180 kg/m³). The specimens were reinforced in the longitudinal direction with two ribbed steel bars of a 10 mm diameter. Eleven notches 5 mm wide and 4 mm deep were cut on the bottom surface of the specimens at a distance of 3 cm (Fig. 2) to induce cracks in the selected locations.
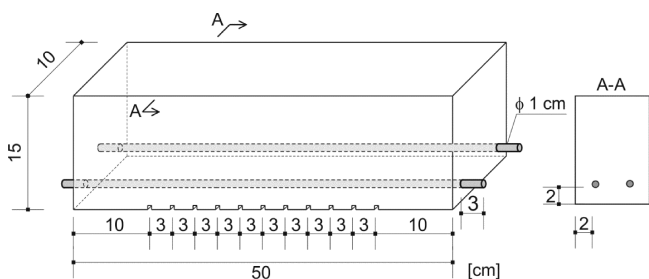

Fig. 2. Geometry and dimensions of the test concrete specimen

3.2. Three-point bending testing. The reinforced concrete specimens were subjected to mechanical degradation in the form of a three-point bending test (Fig. 3a, 3b). The distance between supports was 40 cm and the concentrated force was applied in the middle of the specimen. The bending test was carried out in the testing machine Zwick/Roell Z400 using displacement control with a speed of the cross-head of 0.1 mm/min. The test was stopped when the force reached a value of 50 kN. The force range was selected to achieve a quasi-linear force-displacement relationship and to induce cracks having ability to close after unloading. The tests were

carried out on two concrete specimens of the same geometry: specimen #1 and specimen #2. The displacement of the cross-head and the force level was recorded during the test. The duration of the bending test was 1275 s for specimen #1 and 1305 s for specimen #2. The maximum displacement of the cross-head was 2.12 mm for specimen #1 and 2.17 mm for specimen #2. Figure 4 shows the force-displacement (P–u) and the force-time (P–t) curves for the tested specimens. After the initial stage (displacement range from 0 mm to about 0.9 mm) which corresponds to the adjustment of the sample to the supports, the relationship between the force and the displacement is approximately linear.
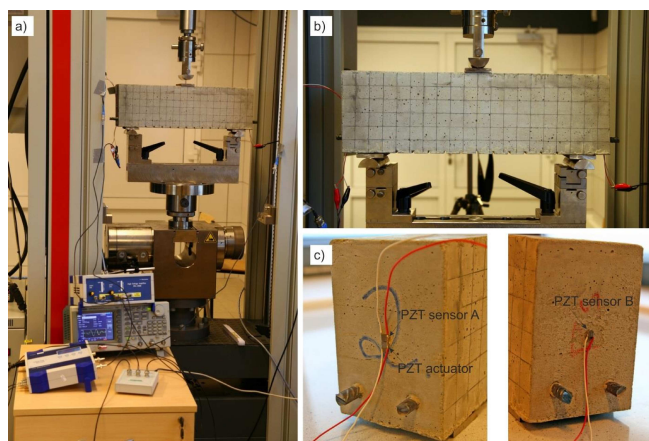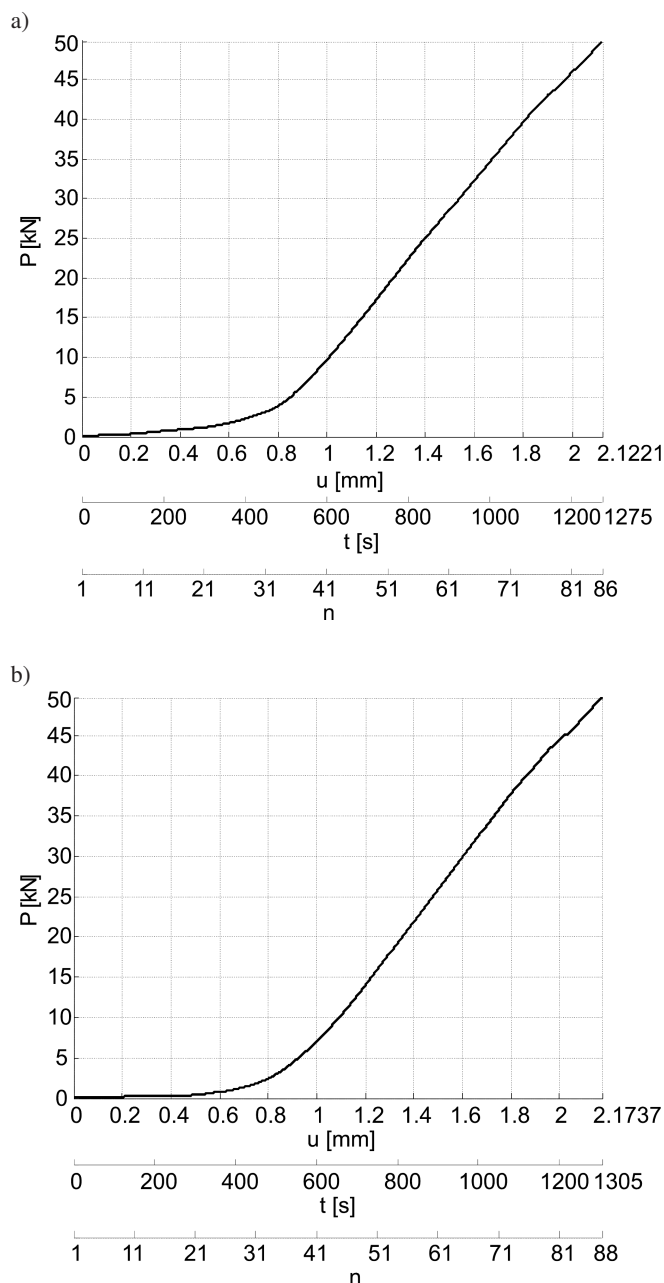

Fig. 3. Experimental set-up for combined bending and ultrasonic tests in the concrete specimen: a) photograph of instrumentation; b) the specimen under three-point bending; c) details showing location of the PZT actuator and the PZT sensors on the specimen

Fig. 4. Experimental force-deflection (P–u) and force-time (P–t) curves registered by the testing machine: a) specimen #1; b) specimen #2

M. Rucka and K. Wilde

3.3. Ultrasonic testing. The experimental setup for the wave propagation is shown in Fig. 3a. The arbitrary waveform generator (Tektronix AFG 3022) with the high voltage amplifier (EC Electronics PPA 2000) generated ultrasonic waves which were acquired by the digital oscilloscope (ScopeDAQ) with a sampling frequency of 1 MHz. The PZT plate actuators Noliac CMAP11 of dimensions $5\times5\times2$ mm were used both as actuator and sensors. The PZT actuator was bonded at one end of the concrete specimen and two PZT sensors (sensors A and B) at both ends of the concrete specimen (Fig. 3c). Petro wax was uses as a coupling agent. The PZT actuator produced an ultrasonic wave which propagated through the concrete specimen in the longitudinal direction. The excitation signal was chosen as a wave packet – a product of a sinusoidal function of frequency f and a window function $w(t)$:

$$p(t) = \begin{cases} p_o \sin(2\pi f t) \cdot w(t) & t \in [0, T_w], \\ 0 & t > T_w, \end{cases} \quad (1)$$

where T_w denotes the length of a window and p_o is an amplitude of the sinusoidal function.

The window function provides the smoothed tone burst in order to reduce the excitation of side frequencies [22]. The Hanning window is most often used for guided wave propagation purposes because it generates the smallest side lobes around the carrier frequency. The Hanning window is described by the equation:

$$w(t) = 0.5 \left(1 - \cos\left(2\pi f t / n_w\right)\right), \qquad t \in [0, T_w], \quad (2)$$

where n_w is the number of counts in the tone burst. The frequency of the applied sine wave influences the width of the main beam in the frequency domain. For a fixed number of counts in the tone burst, low frequency is advantageous to obtain a narrow band in the frequency domain, but simultaneously the wave packet length increases in the time domain. However, high frequency increases the width of the main beam in the frequency domain and decreases the wave packet length in the time domain. For the tested reinforced concrete samples the value of n_w was set as 4 and the frequency of wave was selected as 96 kHz to compromise the acceptable resolution level in both time and frequency domains.

4. Procedures of combined bending-ultrasonic test

While the specimens were subjected to bending by gradually increasing loading, the ultrasonic waves were generated to propagate through the material. The time signals of ultrasonic waves were taken automatically at points A and B each 15 seconds and an ordinal number was assigned for each waveform. An integer parameter n was introduced, starting from $n = 1$ and reaching $n = 86$ for specimen #1 and $n = 88$ for specimen #2. The first measurement ($n = 1$) was made at the unloaded stage. For specimen #2 additional measurements were taken at the end of the bending test. The ultrasonic signals of numbers $n = 89$–90 were registered for the specimen subjected to a 50 kN load, while the signals of numbers $n = 91$–93 were registered after unloading.

Photographs were taken to observe the damage evolution at the front side of the specimen, tracing the bending tests entirely. Figures 5 and 6 present the crack formation in tested specimens #1 and #2, respectively at the increasing load levels. At the first stage of the fracture process, a vertical crack started to develop at the bottom of the specimen. The single crack was initiated at $t = 855$ s ($n = 58$) for specimen #1 and at $t = 840$ s ($n = 57$) for specimen #2. Next cracks began to appear and develop within the prism. At the last stage of damage cracks had length up to 5/6 of the specimen height. It occurred at $t = 1275$ s ($n = 86$) for specimen #1 and at $t = 1305$ s ($n = 88$) for specimen #2.
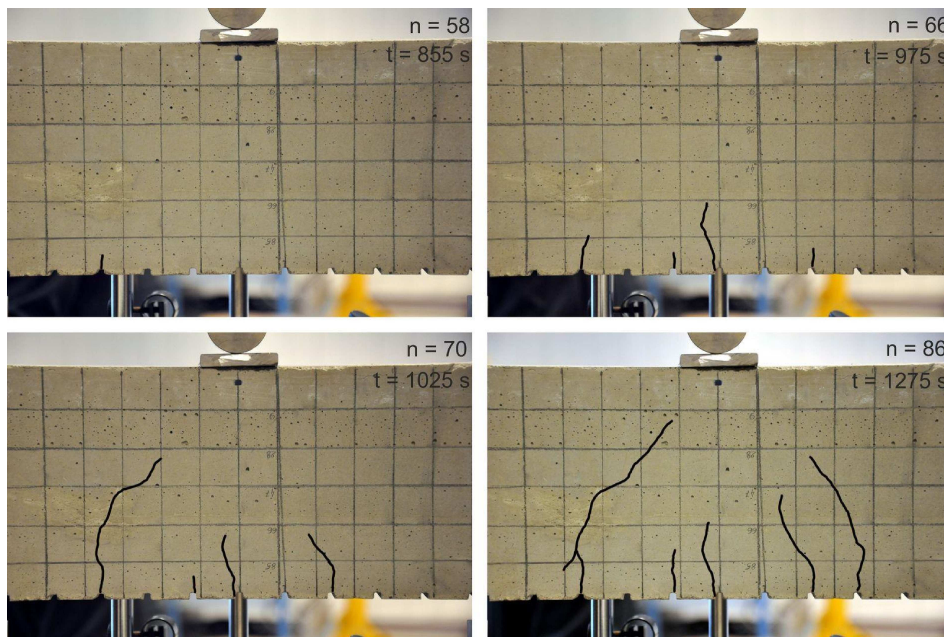

Fig. 5. Experimental damage evolution and crack patterns of specimen #1

Ultrasound monitoring for evaluation of damage in reinforced concrete
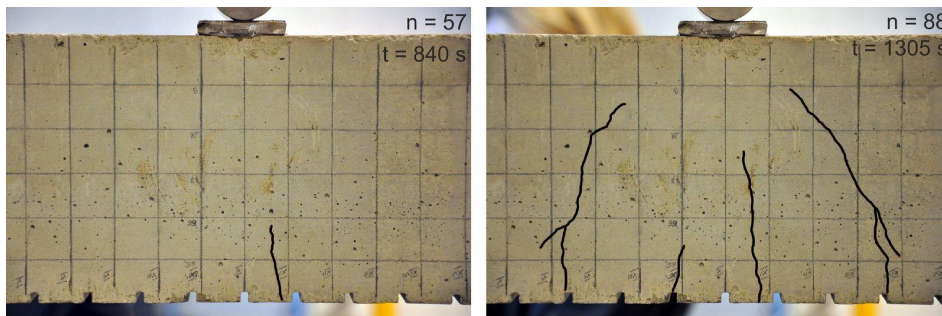

Fig. 6. Experimental damage evolution and crack patterns of specimen #2

The examples of ultrasonic signals acquired at point B for specimen #2 are shown in Fig. 7. It can be seen that no significant differences were visible in the measured time signals at the initial stage of bending (e.g. $n = 1$ and $n = 40$). After cracking, the amplitude of time signals decreased with the external load increment and the progressive stage of damage. After unloading, the amplitude of signals increased indicating the cracks closure (Fig. 7). The comparison of the waveforms for the undamaged stage ($n = 1$), for the stage with one crack of length about 4 cm ($n = 57$) and for the stage with one crack of length about 6 cm ($n = 61$) is shown in Fig. 8. The figure clearly shows that the velocity of the P-wave (the first wave packet observed in Fig. 8) was not sensitive to distributed damage while damage significantly affects amplitude of the registered wave.
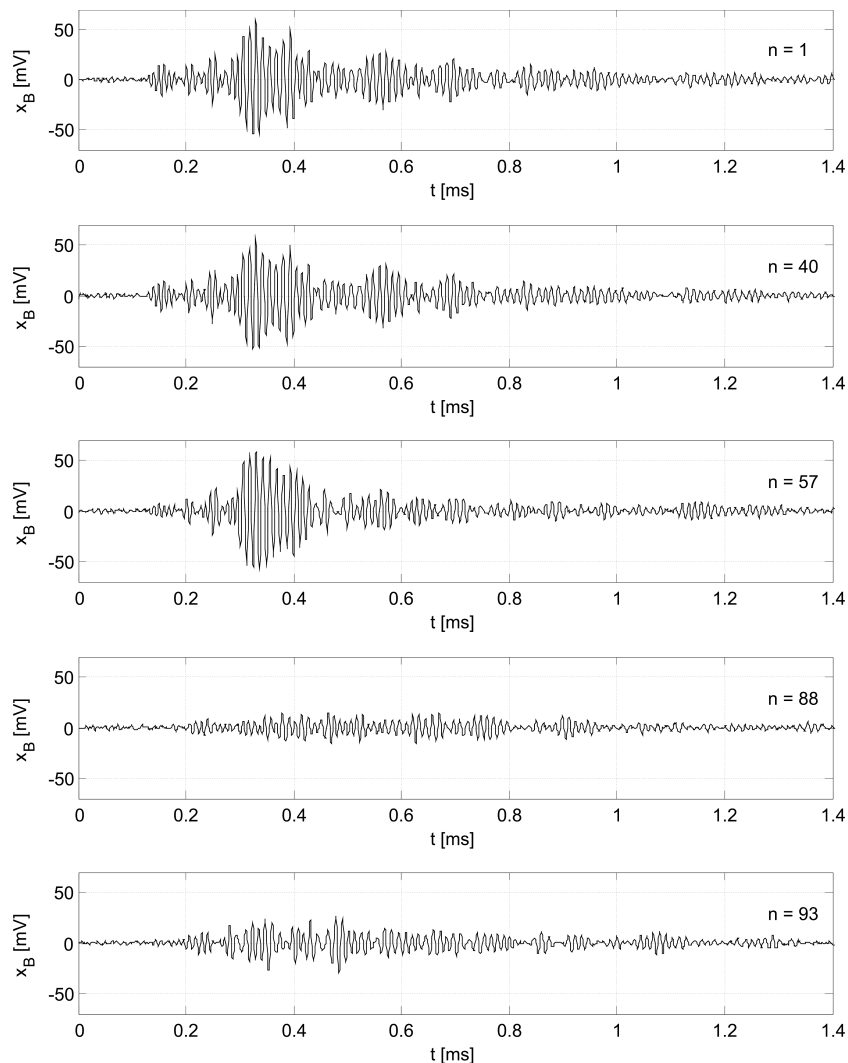

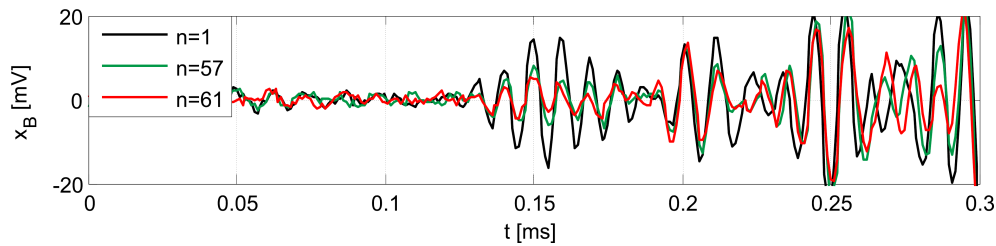Fig. 7. Time signals registered at point B for different load levels for specimen #2

M. Rucka and K. Wilde

Fig. 8. Comparison of time signals registered at point B for specimen #2 for the undamaged stage ($n = 1$), for the stage with a single crack approximately 4 cm long ($n = 57$) and for the stage with a single crack approximately 6 cm long ($n = 61$)

5. Analysis of ultrasound monitoring results and discussion

The analysis of the measured signal x was performed in the frequency domain by means of a power spectral density function. The PSD was estimated with the use of periodogram [23]:

$$G(f) = \frac{2}{f_s N_s} \left| \sum_{n=1}^{N_s} x_n e^{-j(2\pi f/f_s)n} \right|^2, \qquad (3)$$

where f_s is the sampling frequency and N_s is the number of samples.

Time evolution of the frequency spectra for specimens #1 and #2 is shown in Figs. 9 and 10, respectively. The power spectral densities of all ultrasonic signals acquired during the bending test were plotted in the form of maps. Figure 9 illustrates the power spectral densities of the ultrasonic signals measured at point A. All registered waveforms had similar amplitudes because of their close location to the PZT actuator. In the previous tests performed on tensile samples (cf. [21]), a local decrease in the PSD amplitudes of signals measured at point A occurred at the moment of initiation of a first crack as a result of expansion of micro-crack zones around a reinforcing bar. In the present tests on the bending samples this phenomenon did not occur.

The power spectral densities of the signals measured at point B are shown in Fig. 10. At the initial stage of bending (i.e. for ultrasonic signals of numbers n from 1 to about 40), the PSD amplitudes remained at a constant level. Next, the PSD amplitudes decreased with the increase of the damage stage. The rapid decrease of amplitudes can be observed before the appearance of the first vertical crack that was recognised on the photographs. At the moment of the first crack development ($n = 58$ for specimen #1, $n = 57$ for specimen #2), the PSD amplitudes revealed sudden change. We note some nonlinear effects as a frequency shift and generation of an additional frequency peak. This additional frequency component was observable until the crack achieved the length of the half of the beam height. Finally, complete reduction of the PSD amplitudes occurred.
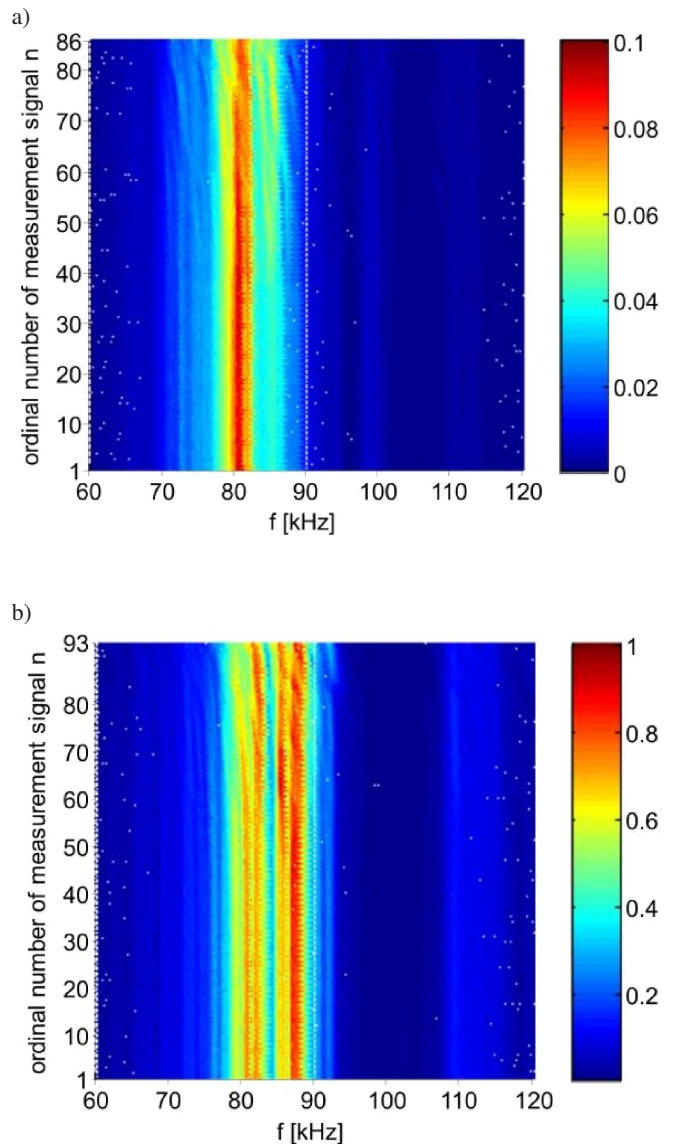
a)

b)

Fig. 9. Power spectral density maps of signals registered at point A: a) specimen #1; b) specimen #2 (power spectral densities are in units of $(\text{mV})^2/\text{Hz}$)
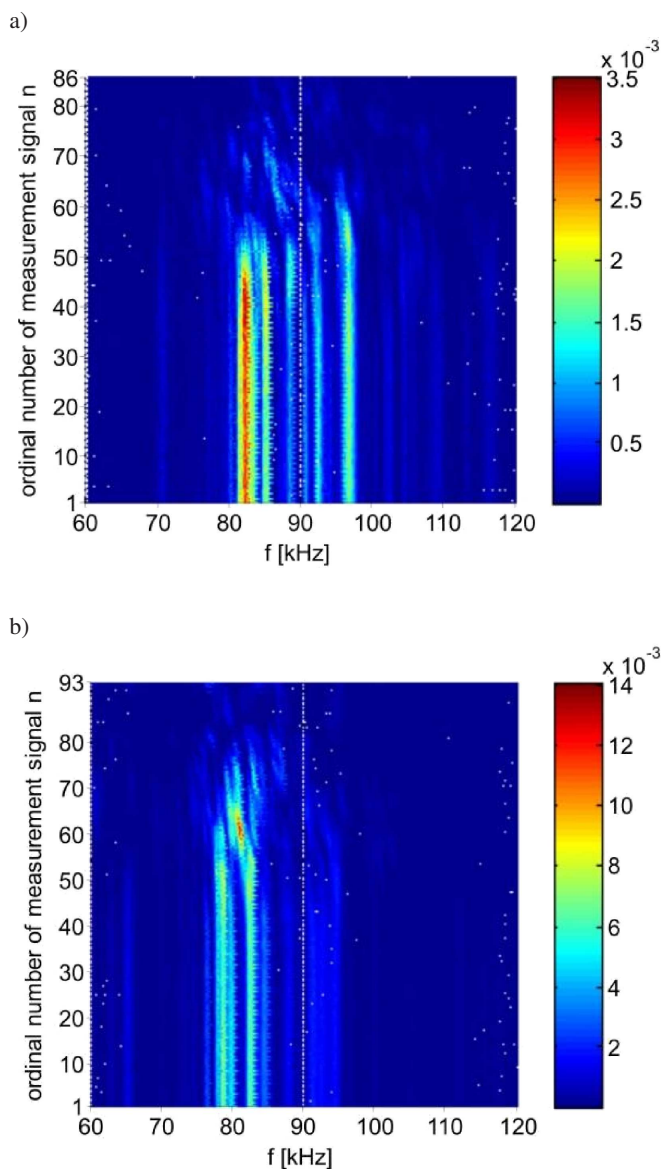
Ultrasound monitoring for evaluation of damage in reinforced concrete

a)

b)

Fig. 10. Power spectral density maps of signals registered at point B: a) specimen #1; b) specimen #2 (power spectral densities are in units of (mV)^2/Hz)
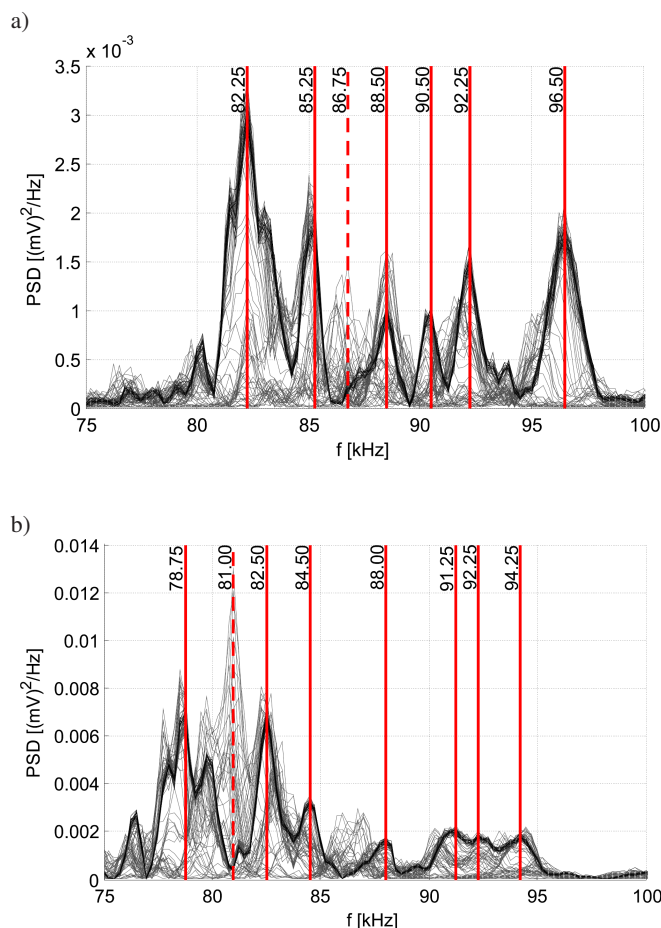
a)

b)

Fig. 11. Power spectral densities of ultrasonic signals registered at point B in the frequency range from 75 kHz to 100 kHz: a) specimen #1; b) specimen #2. Power spectral densities for the first ten signals ($n = 1$–10) are marked with black lines

Figure 11 presents the power spectral density functions of all registered ultrasonic signals. The PSD functions for the first ten signals ($n = 1$–10) are marked with black lines. It can be seen that there are several peaks in the range between 75 kHz and 100 kHz. For specimen#1 six frequencies can be distinguished: 82.25 kHz; 85.25 kHz; 88.5 kHz; 90.5 kHz; 92.25 kHz; 96.5 kHz (Fig. 11a). Similarly, for specimen #2 seven frequencies can be distinguished: 78.75 kHz; 82.5 kHz; 84.5 kHz; 88 kHz; 91.25 kHz; 92.25 kHz; 94.25 kHz (Fig. 11b). The additional frequency components associated with the crack development were marked with the dashed lines (86.75 kHz for specimen #1 and 81 kHz for specimen #2).

Figure 12 depicts the PSD functions of the ultrasonic signals registered at point B in specimen #1 for different load levels. The curves were separated into two graphs for a better visibility. The PSD amplitudes for lower frequency peaks (82.25 kHz; 85.25 kHz; 88.5 kHz) revealed a rapid decrease with similar slope starting with the signal of number $n = 40$ (for the frequency peaks at 82.25 kHz and 85.25 kHz) and $n = 50$ (for the frequency peak at 88.5 kHz). For higher frequency peaks (90.5 kHz; 92.25 kHz; 96.5 kHz) the decrease of the PSD amplitudes did not proceed so regularly. At the moment of initiation of the first surface-breaking crack ($n = 58$), the amplitudes of each peak were significantly lower. Moreover, at this moment, the additional peak at frequency 86.75 Hz was visible and its maximum was for the signal $n = 61$ which corresponds to the stage with three cracks approximately 1 cm long. A further increase in the amplitude of the first two frequency peaks (82.25 kHz and 85.25 kHz) was visible for the signal number about 70, which corresponds to the stage with four cracks.
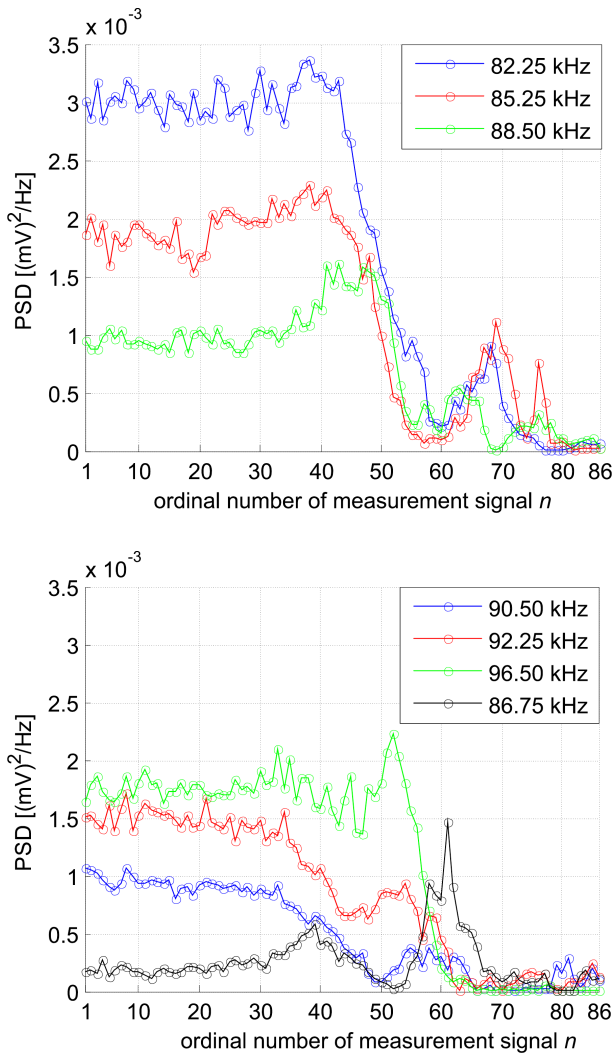
71

Fig. 12. Power spectral densities of ultrasonic signals registered at point B in specimen #1 for different load levels

The PSD results of the ultrasonic signals registered in specimen#2 are illustrated in Fig. 13. The first two frequency peaks (78.75 kHz and 82.5 kHz) revealed a rapid decrease with similar slope starting with the signal of number $n = 50$. The amplitudes of the third peak (84.5 kHz) decreased earlier, starting with the signal of number $n = 40$. At the moment of initiation of the first crack ($n = 57$), the amplitudes of all initially identified PSD peaks were significantly reduced. The additional peak at frequency 81 kHz revealed increase of its amplitude starting with the signal of number $n = 40$ and it reached its maximum value for $n = 60$, which corresponds to the stage with a single crack 6 cm long.

Both tested specimens had slight differences in damage evolution and time histories of registered ultrasonic signals, however, it was possible to observe similar features of their frequency characteristics (Fig. 9 to Fig. 13). The sudden and significant decrease in the PSD amplitudes during formation of micro-crack zones can be regarded as the *distributed micro-crack indicator* DI^m and it can be described by the following relation:

$$DI_n^m(f_i) = \frac{|G_n(f_i) - G_1(f_i)|}{G_1(f_i)}, \tag{4}$$
$$n = 1, 2, ..., N, \qquad i = 1, 2, ..., N_m,$$

where $G_n(f_i)$ is the value of the PSD for the measurement n and frequency f_i, N is the number of registered signals, N_m is the number of frequency peaks existing at the reference state and $G_1(f_i)$ is the reference signal. In both specimens the frequency shift and the generation of additional frequency component appeared after initiation of the first surface-breaking crack. This sudden increase in the PSD amplitudes can be regarded as the *macro-crack indicator* DI_n^M:

$$DI_n^M(f_i^M) = \frac{|G_n(f_i^M) - G_1(f_i^M)|}{G_1(f_i^M)}, \tag{5}$$
$$n = 1, 2, ..., N, \qquad i = 1, 2, ..., N_M,$$

where $G_n(f_i^M)$ is the value of the PSD for the measurement n, f_i^M is the frequency that appears during continuous monitoring of PSD changes. The frequencies f_i^M are not present at the beginning of load application and they appear due to significant damage mechanism that creates new wave propagation patterns.
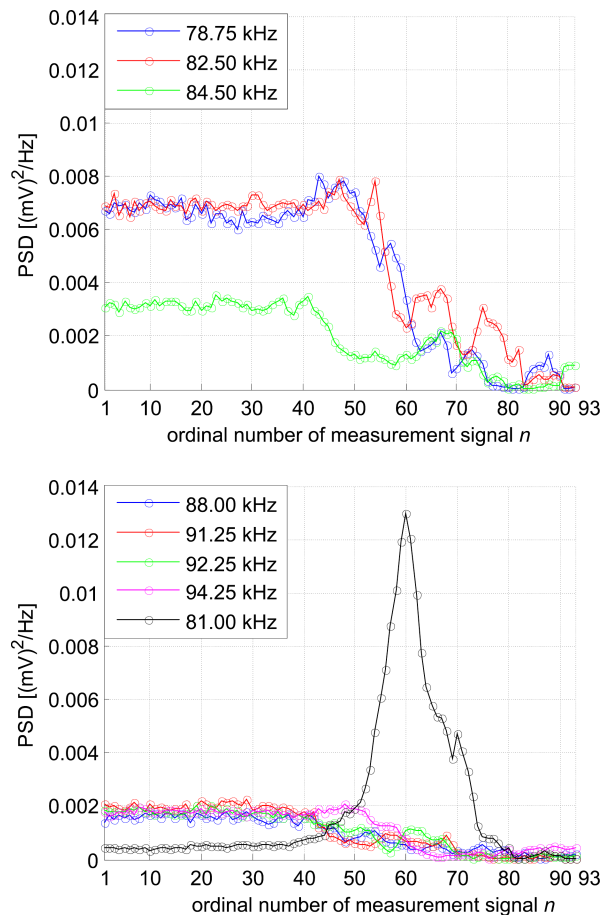

Fig. 13. Power spectral densities of ultrasonic signals registered at point B in specimen #2 for different load levels

The results of the distributed micro-crack indicator DI^m are given in Fig. 14. The indicator values close to zero cor-

respond to the undamaged state while values close to unity indicate damage in the tested specimens. The procedure of automated diagnostics is based on continuous monitoring of the frequency peaks of the PSD functions and computations of $DI^m(f_i)$ indicator for each frequency peak existing at the reference state. The individual values of damage indicator $DI^m(f_i)$ for each frequency peak partially differ from each other (Fig. 14), therefore the mean of all $DI^m(f_i)$ values can be considered as an indicator for the automated diagnostics system:

$$DI_n^m = \left(\sum_{i=1}^{N_m} DI_n^m(f_i) \right) / N_m. \qquad (6)$$

In the case of a value of the distributed micro-crack indicator DI_n^m greater than a preselected threshold (cf. Fig. 14), a warning of the appearance of micro-crack zones is issued. In this study for the tested reinforced concrete samples the threshold value was configured as 0.12. Figure 15 presents the results of the macro-crack indicator DI^M. The appearance of additional frequency peaks is traced and in the case of new f_i^M detected, the indicator DI_n^M is computed. When the macro-crack indicator DI_n^M forms an isolated peak of high amplitude, information on the occurrence of significant internal damage is sent.
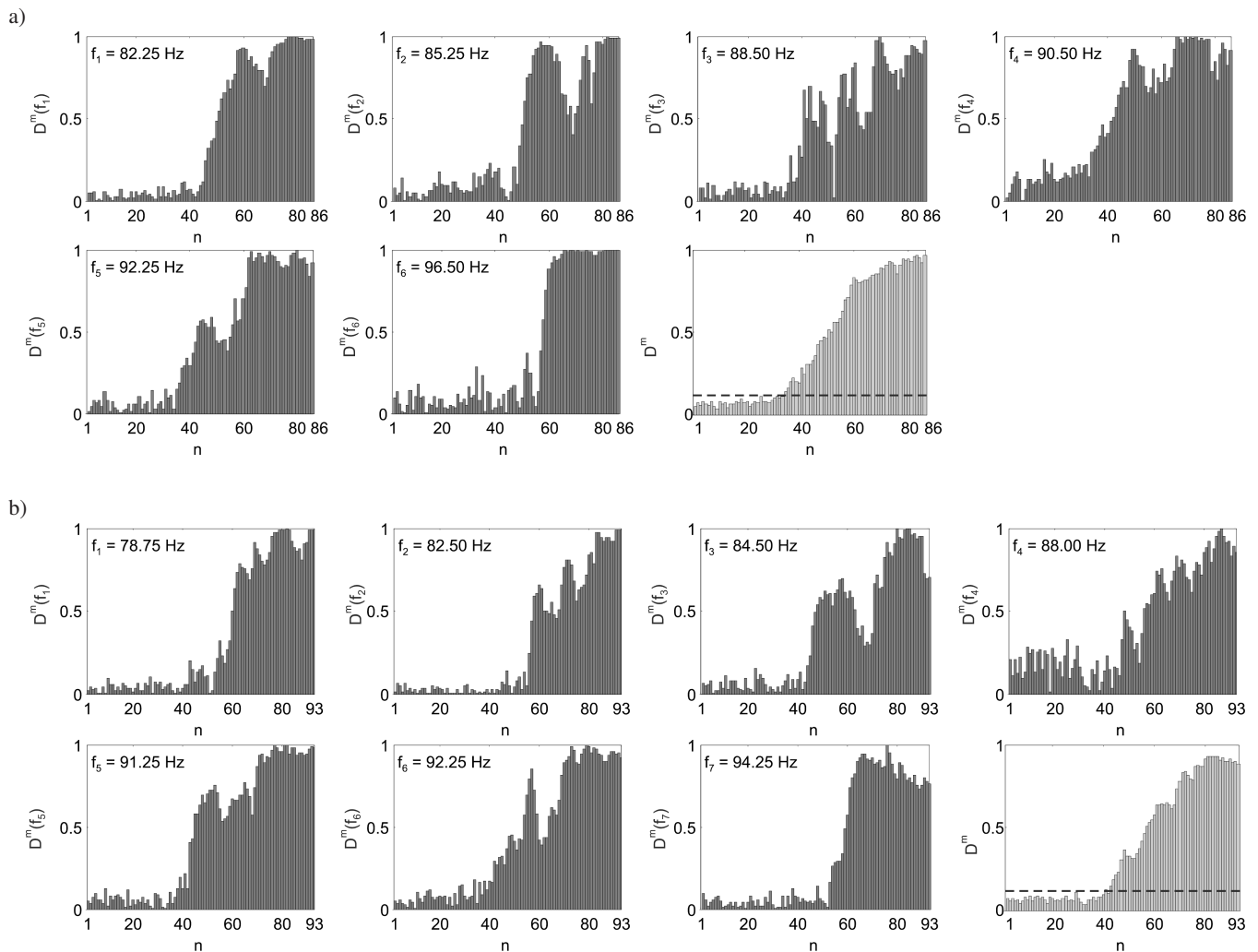

Fig. 14. Distributed micro-crack indicators $DI^m(f_i)$ for frequency peaks existing at the reference state and the mean DI^m of all $DI^m(f_i)$ values: a) specimen #1; b) specimen #2
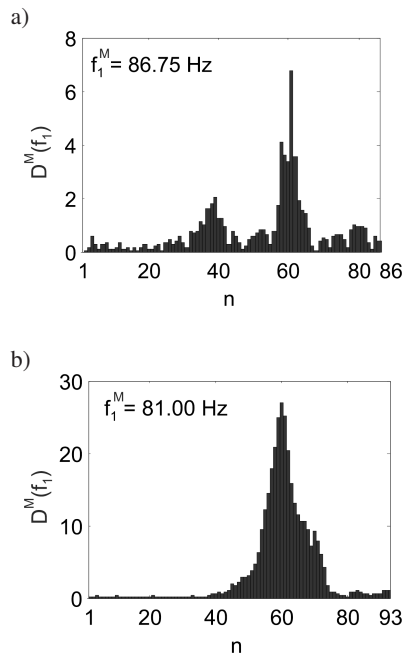
a)

b)

Fig. 15. Macro-crack indicator: a) specimen #1; b) specimen #2

6. Conclusions

The paper presents an experimental study on the possibility of the application of ultrasonic waves for the evaluation and monitoring of distributed micro-cracks and macro-cracks in concrete. The ultrasonic tests were carried out on the reinforced concrete specimens under increasing flexural loading. The analysis of the registered waveforms was performed in the frequency domain with the use of the power spectral density. The applied procedure assumes semi-continuous ultrasonic testing during the element full loading cycle and on-line generation of the PSD maps intended for the assessment of degradation process in the concrete specimens with respect to time.

Damage in the tested specimens was evaluated by the analysis of the reduction of the PSD amplitudes as well as the frequency shifts and generation of the additional frequency components. As a result of the conducted research, two damage indicators were proposed for the assessment of degradation using the proposed automated inspection system. The first damage indicator, called the *distributed micro-crack indicator* is based on a significant reduction of the PSD amplitudes at the stage of the formation of micro-crack zones. It allowed for detection of micro-crack damage before the first visible macro-crack appeared. The second damage indicator, called the *macro-crack indicator* was based on the frequency shift and generation of the additional frequency component in the registered signals. It emerged after formation of the first macro-crack and made detection of surface-breaking cracks at their initial stage of development possible. The experimental results showed that the proposed automated monitoring system based on ultrasonic diagnostics and two damage indicators provided an effective method for the evaluation of progressive damage in concrete.

At this stage of research the study has been limited to diagnostics of reinforced concrete specimens based on two PZT transducers. Such configuration allows to detect damage only within the path of propagating waves without the possibility of precise damage location and damage severity. For automated operation of the monitoring system the threshold value for detection of appearance of micro-crack zones must be set before system activation. The level of the threshold value should be adjusted individually for each structure, according to its importance, used construction material and the severity of operating conditions. The threshold value might be established by an experienced engineer. The selection of the threshold might require experimental tests on structural element samples subjected to damage loads to describe inelastic behaviour of cracked concrete and the appearance of micro-damage zones.

The presented research has a preliminary character. Further studies should be conducted to verify reliability of the proposed method on a large number of real concrete elements with different concrete recipes, different reinforcement systems and various damage scenarios. Verification of the *distributed micro-crack* and *macro-crack indicators* on comprehensive experimental data should be done.

REFERENCES

[1] D.G. Aggelis and T. Shiotani, "Repair evaluation of concrete cracks using surface and through-transmission wave measurements", *Cement & Concrete Composites* 29, 700–711 (2007).

[2] K. Ohno and M. Ohtsu, "Crack classification in concrete based on acoustic emission", *Construction and Building Materials* 24, 2339–2346 (2010).

[3] H.-D. Yun, W.-C. Choi, and S.-Y. Seo, "Acoustic emission activities and damage evaluation of reinforced concrete beams strengthened with CFRP sheets", *NDT&E Int.* 43, 615–628 (2010).

[4] L. Gołaski, B. Goszczyńska, G. Świt, and W. Trąmpczyński, "System for the global monitoring and evaluation of damage processes developing within concrete structure under service load", *The Baltic J. Road and Bridge Engineering* 7, 237–245 (2012).

[5] M.R. Clark, D.M. McCann, and M.C. Forde, "Application of infrared thermography to the non-destructive testing of concrete and masonry bridges", *NDT&E Int.* 36, 265–275 (2003).

[6] C.-C. Cheng, T.-M. Cheng, and C.-H. Chiang, "Defect detection of concrete structures using both infrared thermography and elastic waves", *Automation in Construction* 18, 87–92 (2008).

[7] V. Pérez-Gracia, F. García García, and I. Rodriguez Abad, "GPR evaluation of the damage found in the reinforced concrete base of a block of flats: A case study", *NDT&E Int.* 41, 341–353 (2008).

[8] J. Hugenschmidt, A. Kalogeropoulos, F. Soldovieri, and G. Prisco, "Processing strategies for high-resolution GPR concrete inspections", *NDT&E Int.* 43, 334–342 (2010).

[9] B.H. Hertlein, "Stress wave testing of concrete: A 25-year review and a peek into the future", *Construction and Building Materials* 38, 1240–1245 (2013).

[10] S. Iyer, S.K. Sinha, M.K. Pedrick, and B.R. Tittmann, "Evaluation of ultrasonic inspection and imaging systems for concrete pipes", *Automation in Construction* 22, 149–164 (2012).

[11] J. Hoła, Ł. Sadowski, and K. Schabowicz, "Nondestructive identification of delaminations in concrete floor toppings with acoustic methods", *Automation in Construction* 20, 799–807 (2011).

[12] Y. Yang, G. Cascante, and M.A. Polak, "Depth detection of surface-breathing crack in concrete plates using fundamental Lamb modes", *NDT&E Int.* 42, 501–512 (2009).

[13] P. Antonaci, C.L.E. Bruno, A.S. Gliozzi, and M. Scalerandi, "Monitoring evolution of compressive damage in concrete with linear and nonlinear ultrasonic methods", *Cement and Concrete Research* 40, 1106–1113 (2010).

[14] A.A. Shah and Y. Ribakov, "Damage detection in concrete using nonlinear signal attenuation ultrasound", *Latin American J. Solids and Structures* 9, 713–730 (2012).

[15] H.J. Yim, J. H. Kim, S.-J. Park, and H.-G. Kwak, "Characterization of thermally damaged concrete using a nonlinear ultrasonic method", *Cement and Concrete Research* 42, 1438–1446 (2012).

[16] M. Molero, S. Aparicio, G. Al-Assadi, M.J. Casati, M.G. Hernández, and J.J. Anaya, "Evaluation of freeze–thaw damage in concrete by ultrasonic imaging", *NDT&E Int.* 52, 86–94 (2012).

[17] C.-W. In, R. B. Holland, J.-Y. Kim, K.E. Kurtis, L.F. Kahn, and L.J. Jacobs, "Monitoring and evaluation of self-healing in concrete using diffuse ultrasound", *NDT & E Int.* 57, 36–44 (2013).

[18] H. Su, J. Hu, J. Tong, and Z. Wen, "Rate effect on mechanical properties of hydraulic concrete flexural-tensile specimens under low loading rates using acoustic emission technique", *Ultrasonics*, 52, 890–904 (2012).

[19] Y. Li, C.-e. Sui and Q.-j. Ding, "Study on the cracking process of cement-based materials by AC impedance method and ultrasonic method", *J. Nondestructive Evaluation* 31, 284–291 (2012).

[20] R.S. Adhikari, O. Moselhi, and A. Bagchi, "Image-based retrieval of concrete crack properties for bridge inspection", *Automation in Construction* 39, 180–194 (2014).

[21] M. Rucka and K. Wilde, "Experimental study on ultrasonic monitoring of splitting failure in reinforced concrete", *J. Nondestructive Evaluation* 32, 372–383 (2013).

[22] V. Giurgiutiu, *Structural Health Monitoring with Piezoelectric Wafer Active Sensors*, Academic Press, Amsterdam, 2008.

[23] Signal Processing Toolbox^{TM} run under MATLAB$^{®}$ 7.13 (The MathWorks Inc., Natck, MA, New York).